The Astrophysical Journal Letters, 865:L11 (5pp), 2018 September 20 https://doi.org/10.3847/2041-8213/aadf89
© 2018. The American Astronomical Society. All rights reserved.

Noble Gas Abundance Ratios Indicate the Agglomeration of 67P/Churyumov–Gerasimenko from Warmed-up Ice

O. Mousis[1], T. Ronnet[1], J. I. Lunine[2], A. Luspay-Kuti[3], K. E. Mandt[3], G. Danger[4], F. Pauzat[5], Y. Ellinger[5], P. Wurz[6], P. Vernazza[1], and L. Le Sergeant d'Hendecourt[4]
[1] Aix Marseille Univ, CNRS, CNES, LAM, Marseille, France; olivier.mousis@lam.fr
[2] Department of Astronomy, Cornell University, Ithaca, NY 14853, USA
[3] Johns Hopkins University Applied Physics Laboratory, Laurel, MD, USA
[4] Aix-Marseille Université, PIIM UMR-CNRS 7345, F-13397 Marseille, France
[5] Sorbonne Université, CNRS, Laboratoire de Chimie Théorique, LCT, F-75005 Paris, France
[6] Physikalisches Institut, University of Bern, Sidlerstrasse 5, CH-3012 Bern, Switzerland
Received 2018 July 20; revised 2018 August 27; accepted 2018 September 6; published 2018 September 21

Abstract

The origin of cometary volatiles remains a major open question in planetary science. Comets may have either agglomerated from crystalline ices condensed in the protosolar nebula (PSN) or from amorphous ice originating from the molecular cloud and interstellar medium. Here, based on the recent argon, krypton, and xenon measurements performed by the ROSINA mass spectrometer on board the European Space Agency's *Rosetta* spacecraft in the coma of 67P/Churyumov–Gerasimenko, we show that these noble gas relative abundances can be explained if the comet's building blocks formed from a mixture of gas and H_2O grains resulting from the annealing of pristine amorphous ice (i.e., originating from the presolar cloud) in the PSN. In this scenario, the different volatiles released during the amorphous-to-crystalline ice phase transition would have been subsequently trapped at lower temperatures in stoichiometric hydrate or clathrate hydrate forms by the crystalline water ice generated by the transition. Once crystalline water was completely consumed by clathration in the ∼25–80 K temperature range, the volatile species remaining in the gas phase would have formed pure condensates at lower temperatures. The formation of clathrates hydrates and pure condensates to explain the noble gas relative abundances is consistent with a proposed interstellar origin of molecular oxygen detected in 67P/Churyumov–Gerasimenko, and with the measured molecular nitrogen depletion in comets.

Key words: astrobiology – comets: general – comets: individual (67P/Churyumov–Gerasimenko) – methods: numerical – solid state: volatile

1. Introduction

The origin of cometary volatiles remains a major open question in planetary science. Comets may have either agglomerated from crystalline ices condensed in the protosolar nebula (PSN; Mousis et al. 2016b; Luspay-Kuti et al. 2016) or from amorphous ice originating from the molecular cloud and interstellar medium (ISM; Klinger 1980; Bar-Nun & Laufer 2003; Bar-Nun et al. 2007; Mumma & Charnley 2011; Rubin et al. 2015; Marty et al. 2017). Here, based on the recent argon, krypton, and xenon measurements performed by the ROSINA mass spectrometer on board the European Space Agency's *Rosetta* spacecraft in the coma of 67P/Churyumov–Gerasimenko (67P/C-G; Rubin et al. 2018), we show that these noble gas relative abundances can be explained if the comet's building blocks formed from a mixture of gas and H_2O grains resulting from the annealing of pristine amorphous ice (i.e., originating from the presolar cloud) in the PSN. In this scenario, the different volatiles released during the amorphous-to-crystalline ice phase transition would have been subsequently trapped at lower temperatures in stoichiometric hydrate or clathrate hydrate forms by the crystalline water ice generated by the transition. Once crystalline water was completely consumed by clathration in the ∼25–80 K temperature range, the volatile species remaining in the gas phase would have formed pure condensates at lower temperatures. The formation of clathrates hydrates and pure condensates to explain the noble gas relative abundances is consistent with a proposed interstellar origin of molecular oxygen detected in 67P/C-G (Bieler et al. 2015; Mousis et al. 2016b, 2018), and with the measured molecular nitrogen depletion in comets (Mumma & Charnley 2011; Rubin et al. 2015).

2. Planetesimal Composition Model

Because they are chemically inert, noble gases are key species for tracing the formation conditions in the PSN of icy bodies such as 67P/C-G (Marty et al. 2017; Rubin et al. 2018). To investigate the trapping conditions of Ar, Kr, and Xe in this comet, we used an equilibrium thermodynamic model depicting the composition of the volatile phase incorporated in icy grains as a function of the PSN temperature (Mousis et al. 2012). This model assumes that the volatile phase incorporated in the building blocks of comets is composed of a mixture of pure ices, stoichiometric hydrates (such as NH_3–H_2O hydrate), and multiple guest (MG) clathrate hydrates that form successive crystalline layers at the surface of refractory microscopic grains, due to the cooling of the disk down to 20 K in the outer part of the PSN (see Figure 1). For the composition of the initial gas phase of the disk, we assumed that the abundances of all elements (C, N, O, S, P, Ar, Kr, and Xe) were protosolar (Lodders et al. 2009) and that O, C, and N exist only in the forms of H_2O, CO, CO_2, CH_3OH, CH_4, N_2, and NH_3. The abundances of CO, CO_2, CH_3OH, CH_4, N_2, and NH_3 are then determined from the chosen $CO:CO_2:CH_3OH:CH_4$ and $N_2:NH_3$ gas-phase molecular ratios. Once the abundances of these molecules are determined, the remaining O gives the abundance of H_2O. We have set $CO:CO_2:CH_3OH:CH_4 = 10:30:1.67:1$ and $N_2:NH_3 = 10:1$ in

source: https://doi.org/10.7892/boris.122697 | downloaded: 12.10.2024

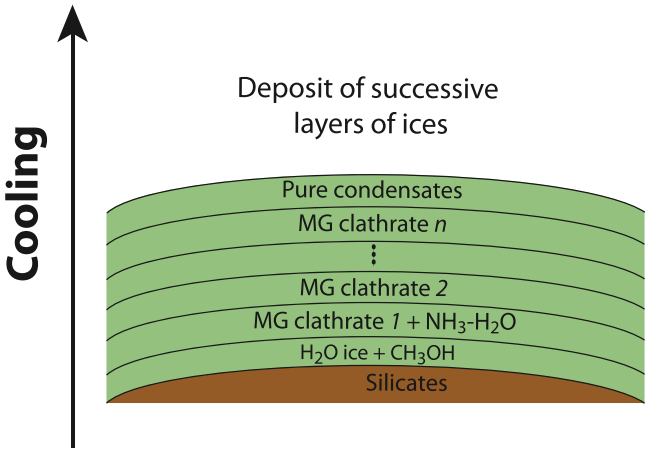

Figure 1. Illustration of the crystallization of the different layers of ices at the surface of refractory grains during the cooling of the disk. The first series of layers composed of H_2O and CH_3OH forms at ∼150 and 100 K, respectively. When the disk's temperature decreases down to ∼80 K and below, several hydrate layers form, including NH_3–H_2O hydrate and clathrate hydrates whose compositions are successively dominated by H_2S and CO_2. Once all of the available water has been consumed by clathration, pure condensates form at temperatures below 25 K (see the text).

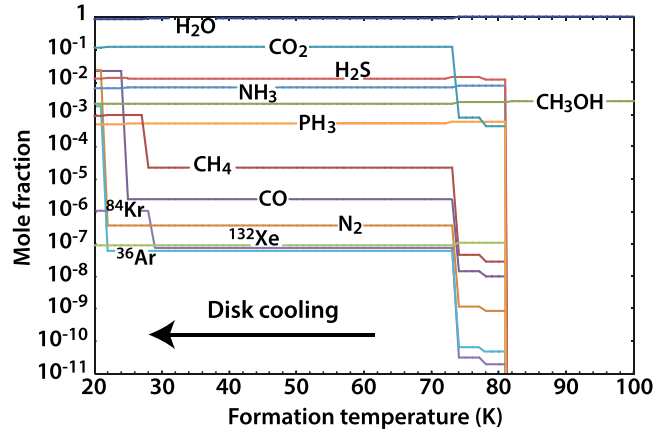

Figure 2. Modeled composition of the volatile phase incorporated in icy grains as a function of their formation temperature during the cooling of the PSN.

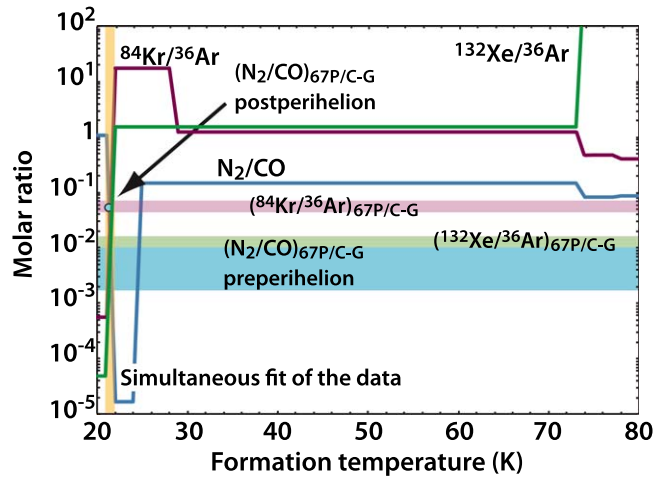

Figure 3. $^{132}Xe/^{36}Ar$, $^{84}Kr/^{36}Ar$, and N_2/CO molar ratios calculated in icy grains as a function of their formation temperature in the outer PSN. The same ratios measured by the ROSINA instrument are shown for the sake of comparison (see the text). The N_2/CO ratio measured in 67P/C-G is represented both before and after perihelion (see the text). The range of N_2/CO pre-perihelion measurements also overlaps with those of $^{132}Xe/^{36}Ar$.

the gas phase of the disk. The $CO:CO_2$ ratio comes from ROSINA observations of the coma of 67P/C-G, from which estimates of the production rates of both CO and CO_2 have been integrated over time and the volume of space sampled between 2014 August and 2016 September (Läuter et al. 2018). The $CO:CH_3OH:CH_4$ ratio is consistent with the production rates measured in the southern hemisphere of 67P/C-G in October 2014 by the ROSINA instrument (Le Roy et al. 2015). The considered $N_2:NH_3$ ratio is predicted by thermochemical models of the PSN (Lewis & Prinn 1980). S is also assumed to exist in the form of H_2S, with $H_2S:H_2 = 0.5 \times (S/H_2)_\odot$, and other refractory sulfide components (Pasek et al. 2005). Finally, CH_3OH is assumed to form only a pure condensate in our calculations because, to the best of our knowledge, no experimental data concerning the equilibrium curve of its associated clathrate hydrate has been reported in the literature.

Our model assumes that the size of these grains grew due to collisional coagulation, which implies no volatile loss during their growth phase (Weidenschilling 1997). A key parameter in the model is that the clathration of volatiles stops when no more crystalline ice is available to trap the volatile species. At this point, the remaining volatiles form only pure condensates at lower disk temperatures. The relative abundances of guest species incorporated in MG clathrate hydrates are determined following a classical statistic mechanics approach linking the thermodynamic properties of clathrate hydrates to the interaction energies and molecular structures (van der Waals & Platteeuw 1959; Lunine & Stevenson 1985; Mousis et al. 2010). We refer the reader to Mousis et al. (2012) for a complete description of the model. We also assume that 67P/C-G accreted late enough to avoid substantial volatile loss during its thermal evolution due to the heat produced by the decay of radiogenic ^{26}Al and ^{60}Fe present in the nucleus. This implies that the comet accreted 2.2–7.7 Myr after the formation of Ca–Al-rich inclusions in the PSN (Mousis et al. 2017a).

3. Results

Figure 2 shows the composition of the volatile phase incorporated into solids agglomerated from ices that formed in the outer PSN, as a function of the disk's temperature during its cooling. In our calculations of the icy phase composition, we considered the same noble gas isotopes as those detected by ROSINA in the coma of 67P/C-G, namely ^{36}Ar, ^{84}Kr, and ^{132}Xe (Balsiger et al. 2015; Rubin et al. 2018). To estimate the protosolar abundances of these elements, we used the Ar, Kr, and Xe isotopic compositions derived from analyses of the solar wind (Lodders 2003).

Figure 3 represents the $^{84}Kr/^{36}Ar$, $^{132}Xe/^{36}Ar$, and N_2/CO ratios in ices formed in the outer PSN as a function of the evolution of the disk's temperature, compared with the same ratios measured in 67P/C-G. The $^{84}Kr/^{36}Ar$ and $^{132}Xe/^{36}Ar$ ratios measured in 67P/C-G, namely 0.058 ± 0.013 and 0.013 ± 0.003, were derived from the analysis of post-perihelion ROSINA data obtained in 2016 May (Rubin et al. 2018). The only range of N_2/CO ratios measured in the coma of 67P/C-G and published so far, namely $(0.17–1.6) \times 10^{-2}$,

comes from ROSINA data acquired before perihelion in 2014 October (Balsiger et al. 2015) and is represented for the sake of comparison in Figure 3. Because these data have not been acquired over the same time period as ^{36}Ar, ^{84}Kr, and ^{132}Xe, we also show in Figure 3 an N_2/CO ratio ($\sim 5.6 \times 10^{-2}$) estimated from the N_2/H_2O and CO/H_2O ratios derived from ROSINA observations in 2016 May (Läuter et al. 2018; Rubin et al. 2018). While this inferred N_2/CO ratio is likely more representative of 67P/C-G's post-perihelion value, it must be taken with caution given the lack of published measurements.

As shown in Figure 2, the three noble gases begin to incorporate into the icy phase at ~80 K in an MG clathrate hydrate dominated by H_2S. The ^{84}Kr/^{36}Ar and ^{132}Xe/^{36}Ar ratios remain constant in the ~29–72 K and ~22–72 K ranges, respectively. Below 22 K, these two ratios drop significantly with very steep slopes, as a result of the incorporation of large amounts of solid Ar in the icy phase. The propensity of Ar for trapping in clathrate hydrate is very poor compared to Kr and Xe[24], so essentially most of it would form pure condensate at low temperature in the PSN. Similarly to Ar, Kr, and Xe, CO and N_2 start their entrapment in clathrate hydrates at ~80 K. The N_2/CO ratio forms a plateau in the ~24–72 K range, and suddenly decreases at temperatures below 24 K. The reason for this decrease is that large amounts of solid CO form at 24 K. Two parameters lead to the formation of solid CO: (i) the lack of available crystalline water that was used up to form the other clathrate hydrates at higher temperatures, and (ii) the lower propensity of CO for entrapment in clathrate hydrates compared to Kr, Xe, CO_2, H_2S, PH_3, and CH_4. Finally, the N_2/CO ratio increases rapidly at disk temperatures of ~22 K, due to the condensation of solid N_2, whose behavior is similar to that of CO.

Figure 3 shows that the ^{84}Kr/^{36}Ar, ^{132}Xe/^{36}Ar, and N_2/CO ratios simultaneously intercept the measured ratios in a narrow temperature range centered around 21–22 K. Interestingly, the N_2/CO ratio varies so steeply that it matches both the pre- and post-perihelion values. While the quality of this matching strongly depends on the reliability of the data, i.e., how representative they are of the comet's bulk's composition, it suggests that the present-day composition of 67P/C-G may be explained by its agglomeration from a mixture of clathrate hydrates with low-temperature ices such as solids of Ar, CO, and N_2 under the thermodynamic conditions of the PSN.

4. Formation of 67P/Churyumov–Gerasimenko

An important constraint on the origin of 67P/C-G's building blocks is the strong correlation between the production rates of O_2 and H_2O observed by the ROSINA instrument (Bieler et al. 2015). This correlation may imply that these two molecules originate from the sublimation of the same icy phase when the comet approaches perihelion. This O_2 would have been likely produced in the presolar cloud or in the ISM via the radiolysis of icy grains by cosmic rays (Mousis et al. 2016b, 2018). This would indicate that 67P/C-G's water ice never followed any cycle of vaporization/condensation in the PSN prior to agglomeration in the building blocks of 67P/C-G. This would then prevent the formation of the crystalline water ice needed to form clathrate hydrates once the amorphous ice grains originating from the presolar cloud have crossed the PSN snow line at ~150 K.

A plausible mechanism overcoming this problem is depicted in Figure 4. Experiments show that amorphous ice starts to crystallize at temperatures higher than ~130 K at PSN conditions. This amorphous-to-crystalline ice phase transition occurs in solid phase in the 130–150 K range (Bar-Nun et al. 2007), allowing water ice to hold on to the O_2 captured in the voids formed by the cosmic-ray flux (Mousis et al. 2016b). At higher temperatures, water ice vaporizes and then releases the captured O_2. Further condensation of O_2 or its trapping into clathrate hydrate in the PSN would be in disagreement with the ROSINA observations currently available in the literature because of the formation of a solid phase distinct from water ice in 67P/C-G (Mousis et al. 2016b). In our formation scenario, the ice grains' precursors of 67P/C-G are then formed from water ice originating from ISM and that crystallized at the amorphous-to-crystalline transition zone (ACTZ). With time,

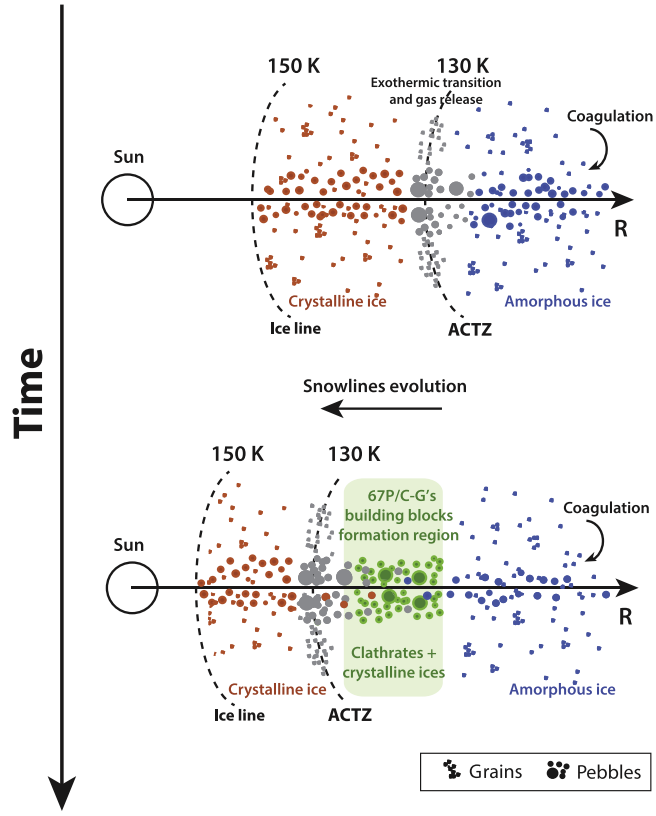

Figure 4. Illustration of the formation conditions of ice grains precursors of 67P/C-G beyond the ice line during the cooling of the PSN. Blue particles: grains/pebbles made from pristine amorphous ice originating from the ISM. Red particles: grains/pebbles made exclusively from crystalline ice condensed at the location of the ice line in the PSN. Gray particles: grains/pebbles made from crystalline ice formed by the amorphous-to-crystalline transition at the location of the ACTZ line. Green particles: grains/pebbles incorporating clathrate hydrates and crystalline ices. Top panel: snapshot of the distribution of grains/pebbles around the different snowlines at a given epoch of the PSN evolution. Small grains coagulate into pebbles that rapidly settle in the midplane and drift inward, thereby allowing pristine material originating from the outer portions of the PSN to be processed in the inner regions. Pebbles made of amorphous water ice crystallize at the ACTZ line and release the adsorbed volatile species as vapors during their inward motion. Crystalline ice also forms from the condensation of water vapor at the ice line that moves inward as the PSN cools. Bottom panel: snapshot of the distribution of grains/pebbles around the different snowlines at a later epoch of the PSN evolution. The snowlines have continued to drift inward as the PSN and clathrate hydrates formed at the surface of grains/pebbles that crystallized from pristine amorphous material at earlier times when the ACTZ line was present at these now cooler locations. With time, these regions of the disk cooled enough to favor the condensation of the most volatile species because the water budget was insufficient to form clathrate hydrates. 67P/C-G likely agglomerated from a mixture of clathrate hydrates and pure condensates formed in these regions.

the disk cooled down due to the decrease of its mass accretion rate onto the Sun (Hartmann et al. 1998), and the ACTZ moved inward, allowing the formation of successive layers of MG clathrate hydrates until pure ices (mainly Ar, CO and N_2) crystallized in the 21–22 K range at the surface of microscopic grains.

As shown in Figure 4, the distributions of solids look very close at the two epochs of the PSN evolution because the coagulation of grains and pebbles drift are processes occurring during the whole lifetime of the disk (see e.g., Birnstiel et al. 2012 for details). However, the coagulation rate progressively decreases with the disk's temporal evolution because of its progressive clearance in pebbles, which start from the outer regions. The solids accreted by 67P/C-G should either result (i) from the agglomeration of local grains that stayed micron-sized during a long time, a requirement for their survival in the outer regions, or (ii) from pebbles that formed at much higher heliocentric distances and that took a long time to coagulate and drift until 67P/C-G's formation region, or (iii) from the two coexisting processes.

5. Discussion and Conclusions

The clathrate hydrate composition predicted by our thermodynamic model depends on the assumptions made regarding the predefined gaseous mixture. The propensity for trapping of a minor species in a clathrate hydrate structure is related to the nature of the dominant species at given pressure and temperature, and weakly depends on the presence of other minor species that are mutually blind to each other. Results similar to those shown in the present work can be obtained as long as CO_2 remains the dominating species in the MG clathrate hydrate, i.e., for any CO_2/CO ratio $\geqslant 2$ in the PSN gas phase.

Our calculations are based on a statistical thermodynamic approach widely used in the fields of geoscience and industry, and allow derivation of the volatiles relative propensities for trapping in MG clathrate hydrates at lower temperatures than those obtained from experiments. One caveat of this kind of model is the lack of low-temperature thermodynamic data, i.e., in the 40–80 K range, for the equilibrium curves of clathrate hydrates, despite the fact that some data do exist at temperatures and pressures down to $\sim$82 K and 2×10^{-7} bar, respectively (Choukroun et al. 2013). The stability domains of various clathrate hydrates at low-pressure and low-temperature ranges are then fitted to experimental data existing at higher temperatures. Another potential issue is the transferability of the potential parameters fitted from experiments and used in the statistical thermodynamic approach to predict the fractions of trapped species in the MG clathrate hydrates at low-pressure and low-temperature conditions. Also, the formation rates of clathrate hydrates of interest are poorly known at PSN conditions and values have been experimentally reported only at temperatures higher than 200 K (see Table 1 of Mousis et al. 2013 for CO_2 and CH_4 clathrates, for instance). Given the wide range of uncertainties, our study assumes that (i) the clathration efficiency is total, and that (ii) the clathration rate is faster than the cooling rate of the PSN and the coagulation rate of icy grains in the PSN. This implies that guest molecules had the time to diffuse through grain pores before their coagulation into the building blocks of 67P/C-G. If the PSN cooling would be faster than the clathration kinetics, then the untrapped volatiles would remain with gas until the disk's temperature decreases down to the condensation temperatures of their respective pure condensates. In this scenario, because of the proximity of their respective equilibrium curves at low temperature, N_2 and CO would condense at very similar temperatures and the resulting N_2/CO in the building blocks of 67P/C-G would be about one order of magnitude higher than the value observed by the ROSINA instrument (Mousis et al. 2016a). In any case, experiments of clathrate hydrate formation conducted under PSN-relevant thermodynamic conditions from a protosolar-like gaseous mixture will be needed in the future to assess our formation scenario.

Despite these cautions, we estimate that the predictions of our model are fairly reliable. Indeed, our thermodynamic model essentially predicts that N_2 and Ar are poor clathrate formers, a property already established in the clathrate hydrate literature from the fact that these small molecules can diffuse throughout the clathrate hydrates cages and are hardly stabilized (Sloan & Koh 2008). Finally, no other mechanism has been shown to offer satisfying explanation thus far. For instance, amorphous ice experiments currently in the literature are in disagreement with the ROSINA measurements (Mousis et al. 2016a; Rubin et al. 2018), including the ones made from a protosolar composition gaseous mixture (Bar-Nun et al. 2007).

Interestingly, it has been claimed that the S_2 detection in comets (A'hearn et al. 1983; Krishna Swamy & Wallis 1987; Laffont et al. 1998; Kim et al. 2003; Boice & Reylé 2005), and notably in 67P/C-G (Le Roy et al. 2015), is by itself a counter argument against the clathration hypothesis because its short lifetime in cometary coma due to photolysis, typically a few hundred seconds in the gas phase, would prevent its desorption from amorphous ice and its subsequent trapping in clathrate hydrates or condensation at lower PSN temperatures (Calmonte et al. 2016). However, this statement would not apply to comets if, similarly to O_2, S_2 formed from the radiolysis of S-bearing molecules embedded in ice grains. In that case, S_2 would also remain in the voids of the ice matrix, even after crystallization, and it would be released only when the ice matrix sublimates (Mousis et al. 2017b). The absence of correlation observed by the ROSINA instrument between the S_2 and H_2O production rates (Calmonte et al. 2016), if this measurement is correct given the extremely small S_2 production rate, would only preclude the trapping of S_2 in a dominant ice reservoir (H_2S clusters could also be embedded within the initially amorphous ice matrix).

We also note that the S_2 production rate was extremely small, and that the outgassing pattern and the correlations between species can show drastic variations on different timescales (e.g., days versus months) depending on when and where the measurements were taken (Hässig et al. 2015; Luspay-Kuti et al. 2015). Therefore, a carefully resolved extended temporal and geographical study of the S_2–H_2O correlation may yield different results than those discussed in previous works (Calmonte et al. 2016). The same applies to the other cometary volatiles, including O_2. A strong correlation between O_2 and H_2O throughout the entire *Rosetta* mission would further strengthen the conclusions of this Letter.

This work is dedicated to the memory of our colleague Daniel Gautier, whose seminal ideas continue to feed current research in solar system formation and the origin of giant planets. O.M. acknowledges support from CNES. O.M. and T.R.

acknowledge support from the A*MIDEX project (n° ANR-11-IDEX-0001-02) funded by the "Investissements d'Avenir" French Government program, managed by the French National Research Agency (ANR). J.I.L. was supported by the *James Webb Space Telescope* project through a grant from NASA/GSFC.

ORCID iDs

A. Luspay-Kuti https://orcid.org/0000-0002-7744-246X
K. E. Mandt https://orcid.org/0000-0001-8397-3315
P. Wurz https://orcid.org/0000-0002-2603-1169

References

A'hearn, M. F., Schleicher, D. G., & Feldman, P. D. 1983, ApJL, 274, L99
Balsiger, H., Altwegg, K., Bar-Nun, A., et al. 2015, SciA, 1, e1500377
Bar-Nun, A., & Laufer, D. 2003, Icar, 161, 157
Bar-Nun, A., Notesco, G., & Owen, T. 2007, Icar, 190, 655
Bieler, A., Altwegg, K., Balsiger, H., et al. 2015, Natur, 526, 678
Birnstiel, T., Klahr, H., & Ercolano, B. 2012, A&A, 539, A148
Boice, D. C., & Reylé, C. 2005, HiA, 13, 501
Calmonte, U., Altwegg, K., Balsiger, H., et al. 2016, MNRAS, 462, S253
Choukroun, M., Kieffer, S. W., Lu, X., et al. 2013, in The Science of Solar System Ices, Astrophysics and Space Science Library, Vol. 356, ed. S. M. Gudipati & J. C. Castillo-Rogez (New York: Springer), 409
Hartmann, L., Calvet, N., Gullbring, E., & D'Alessio, P. 1998, ApJ, 495, 385
Hässig, M., Altwegg, K., Balsiger, H., et al. 2015, Sci, 347, aaa0276
Kim, S. J., A'Hearn, M. F., Wellnitz, D. D., Meier, R., & Lee, Y. S. 2003, Icar, 166, 157
Klinger, J. 1980, Sci, 209, 271
Krishna Swamy, K. S., & Wallis, M. K. 1987, MNRAS, 228, 305
Laffont, C., Boice, D. C., Moreels, G., et al. 1998, GeoRL, 25, 2749
Läuter, M., Kramer, T., Rubin, M., & Altwegg, K. 2018, MNRAS, submitted (arXiv:1804.06696)
Le Roy, L., Altwegg, K., Balsiger, H., et al. 2015, A&A, 583, A1
Lewis, J. S., & Prinn, R. G. 1980, ApJ, 238, 357
Lodders, K. 2003, ApJ, 591, 1220
Lodders, K., Palme, H., & Gail, H.-P. 2009, LanB, 4B, 712
Lunine, J. I., & Stevenson, D. J. 1985, ApJS, 58, 493
Luspay-Kuti, A., Hässig, M., Fuselier, S., et al. 2015, A&A, 583, A4
Luspay-Kuti, A., Mousis, O., Hässig, M., et al. 2016, SciA, 2, 1501781
Marty, B., Altwegg, K., Balsiger, H., et al. 2017, Sci, 356, 1069
Mousis, O., Chassefière, E., Lasue, J., et al. 2013, SSRv, 174, 213
Mousis, O., Drouard, A., Vernazza, P., et al. 2017a, ApJL, 839, L4
Mousis, O., Guilbert-Lepoutre, A., Lunine, J. I., et al. 2012, ApJ, 757, 146
Mousis, O., Lunine, J. I., Luspay-Kuti, A., et al. 2016a, ApJL, 819, L33
Mousis, O., Lunine, J. I., Picaud, S., & Cordier, D. 2010, FaDi, 147, 509
Mousis, O., Ozgurel, O., Lunine, J. I., et al. 2017b, ApJ, 835, 134
Mousis, O., Ronnet, T., Brugger, B., et al. 2016b, ApJL, 823, L41
Mousis, O., Ronnet, T., Lunine, J. I., et al. 2018, ApJ, 858, 66
Mumma, M. J., & Charnley, S. B. 2011, ARA&A, 49, 471
Pasek, M. A., Milsom, J. A., Ciesla, F. J., et al. 2005, Icar, 175, 1
Rubin, M., Altwegg, K., Balsiger, H., et al. 2015, Sci, 348, 232
Rubin, M., Altwegg, K., Balsiger, H., et al. 2018, SciA, 4, eaar6297
Sloan, E. D., & Koh, C. A. 2008, Clathrate Hydrates of Natural Gases (3rd ed.; Boca Raton, FL, London: CRC Press, Taylor and Francis)
van der Waals, J. H., & Platteeuw, J. C. 1959, Clathrate Solutions, Advances in Chemical Physics, Vol. 2 (New York: Interscience), 1
Weidenschilling, S. J. 1997, Icar, 127, 290